Cellular/Molecular

G-Protein-Coupled Receptor Modulation of Striatal $Ca_V1.3$ L-Type Ca^{2+} Channels Is Dependent on a Shank-Binding Domain

Patricia A. Olson,[1] Tatiana Tkatch,[1] Salvador Hernandez-Lopez,[1] Sasha Ulrich,[1] Ema Ilijic,[3] Enrico Mugnaini,[2,3] Hua Zhang,[4] Ilya Bezprozvanny,[4] and D. James Surmeier[1,3]

Departments of [1]Physiology and [2]Cell and Molecular Biology, and [3]Institute for Neuroscience, Feinberg School of Medicine, Northwestern University, Chicago, Illinois 60611, and [4]Department of Physiology, University of Texas Southwestern Medical Center at Dallas, Dallas, Texas 75390

Voltage-gated L-type Ca^{2+} channels are key determinants of synaptic integration and plasticity, dendritic electrogenesis, and activity-dependent gene expression in neurons. Fulfilling these functions requires appropriate channel gating, perisynaptic targeting, and linkage to intracellular signaling cascades controlled by G-protein-coupled receptors (GPCRs). Surprisingly, little is known about how these requirements are met in neurons. The studies described here shed new light on how this is accomplished. We show that D_2 dopaminergic and M_1 muscarinic receptors selectively modulate a biophysically distinctive subtype of L-type Ca^{2+} channels ($Ca_V1.3$) in striatal medium spiny neurons. The splice variant of these channels expressed in medium spiny neurons contains cytoplasmic Src homology 3 and PDZ (postsynaptic density-95 (PSD-95)/Discs large/zona occludens-1) domains that bind the synaptic scaffolding protein Shank. Medium spiny neurons coexpressed $Ca_V1.3$-interacting Shank isoforms that colocalized with PSD-95 and $Ca_V1.3a$ channels in puncta resembling spines on which glutamatergic corticostriatal synapses are formed. The modulation of $Ca_V1.3$ channels by D_2 and M_1 receptors was disrupted by intracellular dialysis of a peptide designed to compete for the $Ca_V1.3$ PDZ domain but not with one targeting a related PDZ domain. The modulation also was disrupted by application of peptides targeting the Shank interaction with Homer. Upstate transitions in medium spiny neurons driven by activation of glutamatergic receptors were suppressed by genetic deletion of $Ca_V1.3$ channels or by activation of D_2 dopaminergic receptors. Together, these results suggest that Shank promotes the assembly of a signaling complex at corticostriatal synapses that enables key GPCRs to regulate L-type Ca^{2+} channels and the integration of glutamatergic synaptic events.

Key words: **L-type channels; $Ca_V1.2$; $Ca_V1.3$; patch clamp; neuromodulation; PDZ domain; state transitions; basal ganglia; dopamine; acetylcholine; PSD-95**

Introduction

Voltage-dependent Ca^{2+} channels perform an astonishing array of specialized functions in neurons. In perisomatic and dendritic regions, L-type Ca^{2+} channels are particularly important in translating synaptic activity into alterations in gene expression and neuronal function. Synaptically driven activation of transcription factors, like cAMP response element-binding protein (CREB) and nuclear factor of activated T-cells, depend on these channels (Murphy et al., 1991; Bading et al., 1993; Graef et al., 1999; Mermelstein et al., 2000; Dolmetsch et al., 2001). L-type Ca^{2+} channels also are key participants in the regulation of long-term alterations in synaptic strength (Bolshakov and Siegelbaum, 1994; Calabresi et al., 1994; Kapur et al., 1998; Yasuda et al., 2003) as well as short-term dendritic excitability, the active processing of synaptic events and repetitive spiking (Avery and Johnston, 1996; Hernandez-Lopez et al., 2000; Bowden et al., 2001; Lo and Erzurumlu, 2002; Vergara et al., 2003).

The engagement of L-type Ca^{2+} channels is regulated by G-protein-coupled receptors (GPCRs). In a variety of excitable cells, GPCRs modulate L-type channel opening by controlling channel phosphorylation state (Hell et al., 1993a; Surmeier et al., 1995; Gao et al., 1997; Kamp and Hell, 2000). In striatal medium spiny neurons, both D_2 dopaminergic and M_1 muscarinic receptors suppress L-type Ca^{2+} channel currents by activating the Ca^{2+}/calmodulin-dependent protein phosphatase calcineurin (Howe and Surmeier, 1995; Hernandez-Lopez et al., 2000). However, it isn't clear whether GPCRs modulate perisynaptic L-type Ca^{2+} channels. Both GPCRs are found in abundance near corticostriatal glutamatergic synapses that are formed preferentially on spine heads in medium spiny neurons (Bolam et al., 2000), where functional studies suggest L-type channels are located (Calabresi et al., 1994; Cepeda et al., 1998).

The physical association that would be necessary for synaptic

Received Aug. 13, 2004; revised Nov. 16, 2004; accepted Dec. 6, 2004.

This work was supported by National Institutes of Health (NIH) Grants NS34696 and DA12958 and a grant from the Picower Foundation to D.J.S. and by grants from the Robert A. Welch Foundation and NIH (NS39552) to I.B. We thank Dr. Richard Miller for providing $Ca_V2.3$ knock-out mice and insight into channel biology. We also acknowledge the expert technical assistance of Karen Burnell and Yu Chen.

Correspondence should be addressed to D. James Surmeier, Department of Physiology, Feinberg School of Medicine, Northwestern University, 303 East Chicago Avenue, Chicago, IL 60611. E-mail: j-surmeier@northwestern.edu.

DOI:10.1523/JNEUROSCI.3327-04.2005

 0270-6474/05/251050-13$15.00/0

GPCR regulation of L-type channels could be created by synaptic scaffolding or adaptor proteins (Kennedy, 1998; Sheng and Kim, 2000). Recent work has shown that L-type Ca^{2+} channels possessing a pore-forming $Ca_V1.2$ subunit bind to several adaptor proteins, and this interaction enables phosphorylated pCREB signaling (Kurschner et al., 1998; Kurschner and Yuzaki, 1999; Weick et al., 2003). This terminal region also associates the channel with signaling enzymes and GPCRs (Davare et al., 2000, 2001). Much less is known about targeting of the other major class of L-type Ca^{2+} channel found in neurons in which the pore is formed by a $Ca_V1.3$ subunit. Unlike $Ca_V1.2$ channels, these channels open at membrane potentials likely to be achieved during modest synaptic stimulation (Koschak et al., 2001; Scholze et al., 2001; Xu and Lipscombe, 2001). The C-terminal region of this subunit is alternatively spliced, yielding long ($Ca_V1.3a$) and short ($Ca_V1.3b$) variants (Safa et al., 2001; Xu and Lipscombe, 2001). The long splice variant contains an Src homology 3 (SH3) and a class I PDZ (postsynaptic density-95 (PSD-95)/Discs large/zona occludens-1) binding domain that selectively binds Shank proteins, which are thought to be key scaffolding elements in the synaptic signaling complex (Kennedy, 1998; Sheng and Kim, 2000). The results presented here suggest that, indeed, Shank targeting of $Ca_V1.3a$ channels enables their selective modulation by dopaminergic and cholinergic GPCRs.

Materials and Methods

Animals. C57BL/6 mice were obtained from Harlan (Indianapolis, IN). $Ca_V1.3$ knock-out mice were obtained from Joerg Striessnig (Institut für Biochemische Pharmakologie, Innsbruck, Austria) (Platzer et al., 2000), rederived, and backcrossed on a C57Bl/6 background in the Northwestern University barrier facility. All experiments followed protocols approved by the Northwestern University Center for Comparative Medicine, an Association for Assessment and Accreditation of Laboratory Animal Care accredited facility, and followed guidelines issued by the National Institutes of Health and the Society for Neuroscience.

Tissue preparation for single neurons. The brain was removed from young (>3–6 weeks of age) male C57BL/6 mice, chilled, sliced (300 μm) coronally in sucrose, and immediately placed in $NaHCO_3$-buffered Earl's balanced salt solution saturated with 95% O_2 and 5% CO_2 where it was held from 20 min to 6 h. The striatum was dissected from the slices immediately before dissociation and placed in HBSS saturated with O_2 and containing type XIV bacterial protease (1 mg/ml) for 25 min. EDTA (0.5 mM) and L-cysteine (1 mM) was added to papain (final concentration, 40 U/ml, pH 7.2) (Raman et al., 2000) for experiments involving D_2, M_1, or 5-HT_2 receptor agonists. Penicillin-streptomycin was added to the papain solution to inhibit bacterial growth. After enzyme digestion, the tissue was triturated for physical dissociation of the medium spiny neurons and then placed in a suspension dish. In some experiments, $Ca_V1.3$ (Platzer et al., 2000) or $Ca_V2.3$ (Wilson et al., 2000) knock-out mice were used for experiments.

Whole-cell voltage-clamp recordings in acutely isolated neurons. Whole-cell recordings used standard techniques (Bargas et al., 1994). The internal solution contained the following (in mM): 180 *N*-methyl-D-glucamine, 40 HEPES, 4 $MgCl_2$, 12 phosphocreatine, 2 Na_2ATP, 0.5 Na_3GTP, and 0.1 leupeptin, pH 7.2–3, with H_2SO_4, 265–270 mOsm/L. A calcium chelator was often omitted; however, for the experiments with dialysis of $Ca_V1.2$ binding peptide into the cell, EGTA (100 μM) was added to the internal. A 2–5 mM Ba^{2+} NaCl external recording solution was used (in mM: 110 NaCl, 1 $MgCl_2$, 2–5 $BaCl_2$, 10 HEPES, 10 glucose, pH 7.35–7.4, 300 mOsm/L). In experiments determining dihydropyridine affinity or voltage dependence of activation, the major salt was tetraethyl-ammonium chloride (135 mM). All drugs were prepared according to the specifications of the manufacturers and applied with a gravity-fed "sewer pipe" capillary array (Surmeier et al., 1995). Electrodes were pulled and fire-polished to 1–2 μm for sufficient resistance in the bath (2–6 MΩ). For acutely isolated recordings, medium spiny neuron morphological identification was supported by a whole-cell capacitance ranging from 2–10 pF. Isolation of calcium currents was possible with the use of tetrodotoxin (TTX; 200 μM) to block sodium currents and CsCl (20 mM) to block potassium currents. All reagents were obtained from Sigma (St. Louis, MO) except GTP (Roche Diagnostic, Indianapolis, IN), TTX (Alomone Labs, Jerusalem, Israel), leupeptin, ω-conotoxin GVIA (Bachem, Torrance, CA), papain (Worthington, Lakewood, NJ), penicillin-streptomycin (Invitrogen, Carlsbad, CA), and ω-agatoxin TK (Peptides International, Louisville, KY). $Ca_V1.2$ COOH-tail and $Ca_V1.3$ Shank-PDZ binding peptides were synthesized by Biosource (Hopkinton, MA). $Ca_V1.2$ COOH-tail peptide sequence was SEEALPDSRSYVSNL, and $Ca_V1.3$ Shank-PDZ binding peptide sequence was EEEDLADEMICITTL. Whole-cell voltage-clamp recordings were obtained with an Axon Instruments (Foster City, CA) 200A patch-clamp amplifier and controlled and monitored with a Macintosh G4 running pulse 8.53 with a 125 KHz interface. Data were analyzed using Igor Pro 4.05, and Systat 5.2 and SigmaStat 3.0 software were used for statistical analysis. For clarity, the capacitance artifacts were suppressed in the figures containing current traces. Box plots were used to represent small sample sizes.

Whole-cell recordings in slices. Slices were obtained as described above and placed for >1 h into an artificial CSF (ACSF) containing the following (in mM): 125 NaCl, 3.5 KCl, 25 $NaHCO_3$, 1.25 Na_2HPO_4, 1 $MgCl_2$, 1.2 $CaCl_2$, 25 glucose, pH 7.3, with NaOH, 300 mOsm/L, saturated with 95% CO_2 and 5% O_2. Thereafter, slices were transferred to a recording chamber and superfused with ACSF at a rate of 3–4 ml/min. Current-clamp recordings were performed on visually identified medium spiny neurons with an infrared video-microscopy system. The pipette solution consisted of the following (in mM): 119 $KMeSO_4$, 1 $MgCl_2$, 0.1 $CaCl_2$, 10 HEPES, 1 EGTA, 12 phosphocreatine, 2 Na_2ATP, 0.7 Na_2GTP, pH 7.2–3, with KOH, 280–300 mOsm/L. Whole-cell recordings were obtained at 32°C.

Single-cell reverse transcription-PCR. Two types of reverse transcription (RT)-PCR profiling were performed. To maximize mRNA yields, some neurons were aspirated without recording. Isolated neurons were patched in the cell-attached mode and lifted into a stream of control solution. Neurons were then aspirated into an electrode containing sterile water. In other experiments, neurons were briefly subjected to recordings before aspiration. In these cases, the electrode recording solution was made nominally RNase free. RT procedure was performed using Superscript First-Strand Synthesis System (Invitrogen) as described previously (Surmeier et al., 1996). Primers for enkephalin (ENK) and upper primer for substance P (SP) were described previously (Surmeier et al., 1996). The lower primer for SP was ATG AAA GCA GAA CCA GGG GTA G (position 838; GenBank accession number D17584), which gave a PCR product of 616 bp. $Ca_V1.2$ mRNA (GenBank accession number NM009781) was detected with a pair of primers GAC AAC TGA CCT GCC CAG AG (position 6763) and GCT GTT GAG TTT CTC GCT GGA (position 7098), which gave a PCR product of 356 bp. $Ca_V1.3$ mRNA (GenBank accession number AJ437291) was detected with a pair of primers CTG ACT CGG GAC TGG TCT ATT C (position 4363) and CTG GAG GGA CAA CTT GGT CAA GCA (position 4718), which gave a PCR product of 379 bp. For detection of $Ca_V1.3$ splice variant mRNAs, a common upper primer TCC GGA CAG CTC TCA AGA TCA AG (position 4616) was used. The lower primer for the long form of $Ca_V1.3$ was GAC GGT GGG TGG TAT TGG TCT GC (position 5058), which gave a PCR product of 465 bp. The lower primer for the short form of $Ca_V1.3$ was GCG GTA GCT CAG GCA GAC AAC TC (position 4932; GenBank accession number AF370009), which gave a PCR product of 306 bp. TH mRNA (GenBank accession number NM012740) was detected with a pair of primers CAG GAC ATT GGA CTT GCA TCT (position 1415) and ATA GTT CCT GAG CTT GTC CTT G (position 1690), which gave a PCR product of 297 bp.

Immunoprecipitation. Rat brain synaptosomal fraction [postnatal day 2 (P2)] was purified as described previously (Maximov et al., 1999) and solubilized in the extraction buffer B containing 1% 3-[(3-cholamidopropyl)dimethylammonio]-1-propanesulfonate as follows (in mM): 137 NaCl, 2.7 KCl, 4.3 Na_2HPO_4, 1.4 KH_2PO_4, 5 EDTA, 5 EGTA, and protease inhibitors, pH 7.2. The lysate was clarified by cen-

trifugation at 100,000 × *g* and incubated for 2 h at 4°C with protein A-Sepharose beads (Amersham Biosciences, Piscataway, NJ) coated with affinity-purified anti-$Ca_V1.3a$ polyclonal antibody (pAb). Beads were pelleted by centrifugation, washed two times in the extraction buffer, and analyzed by Western blotting with guinea pig anti-Shank pAb.

Immunocytochemistry. Rabbit anti-Shank was a generous gift from Dr. Eunjoon Kim (Korea Advanced Institute of Science and Technology, Daejeon, Korea); mouse monoclonal anti-PSD-95 (clone 7E3-IB8) was purchased from Sigma-Aldrich; Alexa Fluor 488- and 568-labeled anti-rabbit and anti-mouse goat IgGs were from Molecular Probes (Eugene, OR). Eight normal C57BL/6 male mice and two $Ca_V1.3$ knock-out mice were deeply anesthetized with sodium pentobarbital (60 mg/kg body weight, i.p.) and transcardially perfused with 0.9% saline, followed by 4% freshly depolymerized paraformaldehyde and 15% saturated picric acid in 0.1 M phosphate buffer (PB), pH 7.4, at 4°C. Brains were dissected out, postfixed at room temperature for 1 h, and cryoprotected in 30% sucrose in PB. Frozen sections were cut in the sagittal and coronal planes at 20 μm on a freezing stage microtome. Free-floating sections were processed for indirect immunofluorescence. Unspecific binding was suppressed in a blocking solution containing 5% normal goat serum (NGS) in PBS with 0.05% Triton X-100 for 1 h at room temperature. Sections were then incubated with primary antibodies diluted in 2% NGS/PBS-0.05 Triton X-100 overnight at 4°C, followed by incubation with fluorescent secondary antibodies for 30 min at room temperature. After rinsing in PBS, sections were mounted with Vectashield (Vector Laboratories, Burlingame, CA). For double labeling, sections were incubated with pairs of primary antibodies (anti-PSD-95/anti-Shank, or anti-PSD-95/anti-$Ca_V1.3a$) and then with pairs of appropriate IgGs tagged with Alexa Fluor 488 and 568. Control sections incubated with normal serum in lieu of the primary antiserum were free of immunolabeling, and $Ca_V1.3a$ knock-out mice did not show any immunoreactivity after incubation with antiserum to $Ca_V1.3a$.

Dissociated striatal neurons were obtained as described above, collected on a polylysine-coated glass slide, and fixed with 4% freshly depolymerized paraformaldehyde in 0.1 M PB, pH 7.4, at 4°C. Slides were immunoreacted as above with rabbit anti-$Ca_V1.3a$ and rabbit anti-Shank, and binding sites were revealed with Alexa Fluor 488 and 568-labeled rabbit and goat IgGs. After coverslipping with Vectashield, slides were analyzed by fluorescence microscopy.

Laser-scanning confocal immunofluorescence microscopy was done on a Nikon Eclipse 800 microscope equipped with a Nikon PCM 2000 Confocal Microscope System (Nikon, Melville, NY). This utilizes an Argon laser (457, 488, 514 nm) and a green HeNe laser (535.5 nm). Standard emission filter 515/530 and bandpass filter 605/632 transmitting light between 589 and 621 nm were used for Argon and HeNe lasers, respectively. The system allowed simultaneous detection as well as sequential detection of orange/red (TCP-1 ring complex; Alexa 568; Texas Red) and green (FITC; Alexa 488; and green fluorescent protein) dyes. Detection parameters for sequential detection were optimized for each dye, and spillover between channels was minimized. Images for analysis were obtained with a Nikon planapochromatic 60× (numerical aperture, 1.4) oil immersion lens. Sequential optical sections were taken at 0.5–2.0 μm intervals in the Z plane to build an image volume in three dimensions on a graphics workstation using commercial software (SIMPLE PCI program; Compix Imaging Systems, Lake Oswego, OR). Software settings for optimal gain and black levels were individually adjusted for each fluoroprobe.

Spatial cross-correlations were computed from aligned, 0.5 μm thick, optical sections. The goal of this analysis was to determine whether there was a consistent spatial relationship between immunofluorescent signal intensity for $Ca_V1.3$, PSD-95, and Shank. Although our analytic approach differed somewhat from that recently described by Li et al. (2004), the approach was conceptually similar. Paired neuropil images for PSD-95/Shank or PSD-95/$Ca_V1.3a$ were imported to Adobe Photoshop (Adobe Systems, San Jose, CA). Here, images were converted from color to grayscale; the files were not manipulated in any other way (e.g., no deconvolution or smoothing). Image intensity files were then imported as two-dimensional matrices into Igor Pro where they were standardized using self-reference. Conventional, spatial cross-correlations between aligned, standardized image matrices (Bendat and Piersol, 1971) were computed on a row pixel by row pixel basis for pixel lags up to the equivalent of 10 μm (column-by-column approach yielded similar results). The two-dimensional cross-correlation was then collapsed by averaging across columns. To obtain a measure of the correlation expected by chance, image rows and columns were shifted four times by a random number (generated from a uniform distribution by Igor Pro) and then the image cross-correlations were recomputed. This is presented as the "shuffled" correlation. This shuffling consistently led to "flat" cross-correlations and gave a measure of the background signal generated by the algorithm.

Results

D_2 dopaminergic and M_1 muscarinic receptors suppress L-type Ca^{2+} channel currents in striatal medium spiny neurons

The vast majority of neurons in the rodent striatum are GABAergic medium spiny neurons (>90%). They can readily be identified by their typically bipolar shape and medium size (see Fig. 2*A*). Virtually all medium spiny neurons express M_1 and M_4 muscarinic receptors, reflecting the prominent role of cholinergic signaling in the functioning of the striatum (Graybiel, 1984; Bernard et al., 1992; Yan et al., 2001). Another key neuromodulator in the striatum is dopamine. The postsynaptic effects of dopamine are mediated mostly by D_1 and D_2 dopaminergic receptors, which are differentially expressed by medium spiny neurons projecting to the substantia nigra and the globus pallidus, respectively (Albin et al., 1989; Gerfen, 1992; Surmeier et al., 1996).

One of the most prominent consequences of D_2 dopaminergic or M_1 muscarinic receptor activation in medium spiny neurons is the suppression of L-type Ca^{2+} channel currents. This is easily seen in whole-cell recordings from acutely isolated medium spiny neurons in the presence of the dihydropyridine agonist S(−)-BayK 8644 (1 μM). BayK 8644 enhances the open probability of L-type channels and slows their deactivation rate, enabling them to be examined in isolation without using blockers for the other Ca^{2+} channels. The slowing of the deactivation kinetics can be seen clearly in Figure 1*A*. In the presence of BayK 8644, the application of the D_2 receptor agonist R(−)-propyl-norapomorphine hydrochloride (NPA; 10 μM) reversibly reduces the amplitude of slow, L-type tail currents in approximately half of all medium spiny neurons (Fig. 1*A*,*B*) (Hernandez-Lopez et al., 2000). The tail currents are shown at higher resolution in the right panel in Figure 1*A*. Typically, NPA reduced tail currents measured 5 ms after the repolarizing step by ~20%. Similarly, application of the muscarinic receptor agonist muscarine (2 μM) reversibly reduced the slow tail currents resulting from L-type channels in medium spiny neurons (Fig. 1*C*,*D*). Both GPCRs bring about their modulation by turning on phospholipase Cβ (PLCβ) isoforms, mobilizing inositol trisphosphate (IP_3) receptor (IP_3R) Ca^{2+} stores and activating the calcium-dependent protein phosphatase calcineurin (Howe and Surmeier, 1995; Hernandez-Lopez et al., 2000).

Medium spiny neurons coexpress $Ca_V1.2$ and $Ca_V1.3$ mRNAs

Although D_2 and M_1 receptor activation suppresses L-type Ca^{2+} channel currents, it is not known whether this modulation is specific to a particular channel subtype. In the brain, L-type channels have either a $Ca_V1.2$ or $Ca_V1.3$ pore-forming subunit (Catterall, 1998). To determine whether one or both of these was expressed in striatal medium spiny neurons, single-cell RT-PCR (scRT-PCR) profiling was performed. Medium spiny neurons were identified by their expression of SP or ENK mRNAs. These two peptides reliably mark the two major populations of medium spiny neurons that form so-called "direct" and "indirect" path-

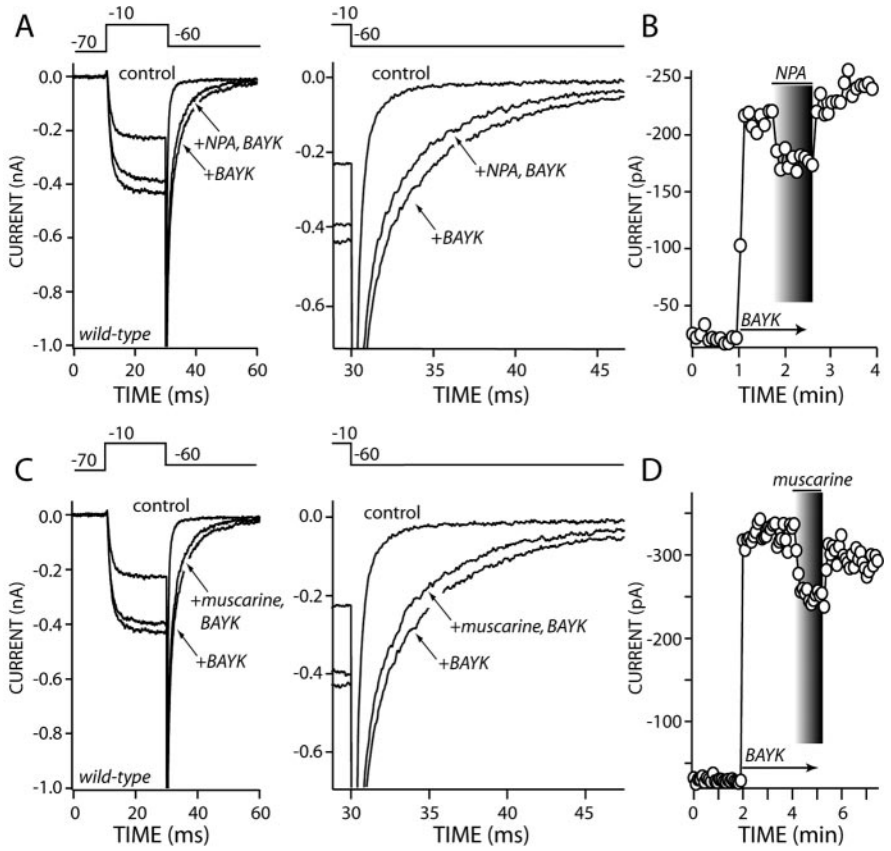

Figure 1. D_2 dopaminergic and M_1 muscarinic receptors inhibit L-type calcium channels in medium spiny neurons. *A*, Control current traces from a dorsal striatal medium spiny neuron from a wild-type mouse: current elicited by S(−)-BayK 8644 (BAYK; 1 μM) alone or with NPA (10 μM). *B*, Measuring the tail current 5 ms after the step isolated L-type current, providing the time course shown. NPA inhibited L-type tail current by 18%. *C*, Control current traces from a dorsal striatal medium spiny neuron from a wild-type mouse: current elicited by BayK 8644 (1 μM) alone or with (+)-muscarine chloride (muscarine; 2 μM). *D*, Measuring the tail current 5 ms after the step isolated L-current, providing the time course shown. Muscarine application inhibited L-type tail currents by 25%.

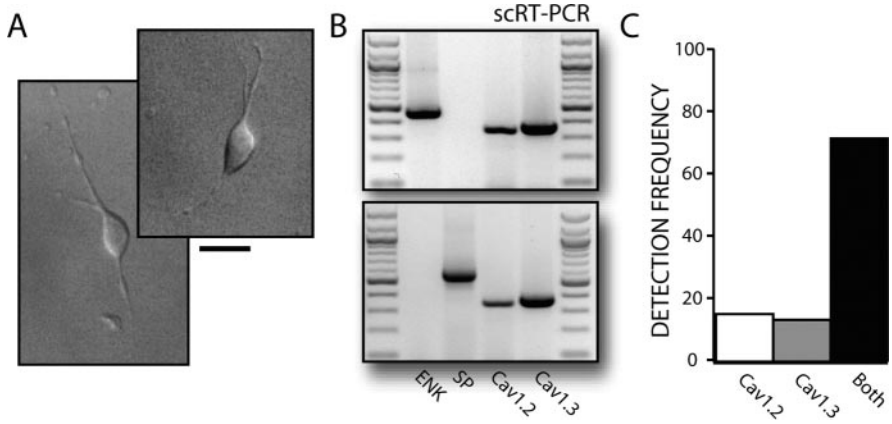

Figure 2. $Ca_V1.2$ and $Ca_V1.3$ mRNAs are coexpressed in striatal medium spiny neurons. *A*, Photomicrograph of two acutely dissociated medium sized neurons from the dorsal striatum. Scale bar, 20 μm. *B*, Single-cell RT-PCR showing both major classes of medium spiny neurons (those expressing SP and those expressing ENK mRNA) coexpress $Ca_V1.2$ and $Ca_V1.3$ mRNA. *C*, Histogram shows that $Ca_V1.2$ and $Ca_V1.3$ mRNA were detected in the majority of the medium spiny neurons profiled ($n = 53$).

ways (Gerfen, 1992). These two populations also differ in their expression of D_1 and D_2 receptors. Because the mRNAs for these peptides have high single-cell copy numbers, they are much more reliable markers in scRT-PCR protocols than low abundance GPCR mRNAs that can easily be missed (Surmeier et al., 1996). These experiments revealed that both SP and ENK neurons coexpressed $Ca_V1.2$ and $Ca_V1.3$ α subunit mRNAs (Fig. 2*B*). $Ca_V1.2$ and $Ca_V1.3$ mRNA were found in >70% of a large sample of medium spiny neurons ($n = 53$) (Fig. 2*C*). Given the probability of false negatives with low-abundance templates at the single-cell level, these results suggest that virtually all medium spiny neurons coexpress $Ca_V1.2$ and $Ca_V1.3$ mRNAs.

$Ca_V1.2$ and $Ca_V1.3$ channels in medium spiny neurons differ pharmacologically and biophysically

In heterologous expression systems, $Ca_V1.2$ and $Ca_V1.3$ channels differ in their affinity for dihydropyridine antagonists (Koschak et al., 2001; Xu and Lipscombe, 2001). To determine whether this distinction was maintained in a native expression system, medium spiny neurons were acutely isolated, voltage clamped using whole-cell techniques, and Ca^{2+} channels were pharmacologically isolated (Bargas et al., 1994). Using Ba^{2+} (5 mM) as a charge carrier to eliminate Ca^{2+}-dependent inactivation, fast (150 ms) voltage ramps running from −80 to +30 mV from a holding potential of −60 mV were used to activate channels (Fig. 3*A*). To better isolate L-type channel currents, $Ca_V2.1/2.2$ channels were blocked (using a combination of ω-conotoxin GVIA and ω-agatoxin TK), leaving just Ca_V1 (L-type) and $Ca_V2.3$ (R-type) channels capable of fluxing ions (Bargas et al., 1994). In this situation, the application of the Ca_V1, L-type channel antagonist nimodipine blocked the evoked current in a dose-dependent manner. Selected traces from one of these experiments are shown in Figure 3*A*. Construction of dose–response plots from wild-type neurons were well fit only with two-site Langmuir isotherm having IC_{50} values near 200 nM and 2 μM ($n = 8$) (data not shown), values close to those obtained for $Ca_V1.2$ and $Ca_V1.3$ channels, respectively, in heterologous expression systems (Koschak et al., 2001; Xu and Lipscombe, 2001). At 10 μM, nimodipine blocked >90% of the current (Fig. 3*A*) with little increase in the block until concentrations reached 50 μM, at which point $Ca_V2.3$ channels began to be blocked (P. A. Olson, R. J. Miller, and D. J. Surmeier, unpublished observations). The low-affinity binding site was preserved in medium spiny neurons from $Ca_V2.3$ knock-out mice (Wilson et al., 2000) ($n = 8$), arguing that there was no confusion with this R-type Ca^{2+} channel. To verify that the high affinity site was attributable to $Ca_V1.2$ channels, medium spiny neurons from $Ca_V1.3$ knock-out mice were examined. As predicted, L-type currents in these neurons were

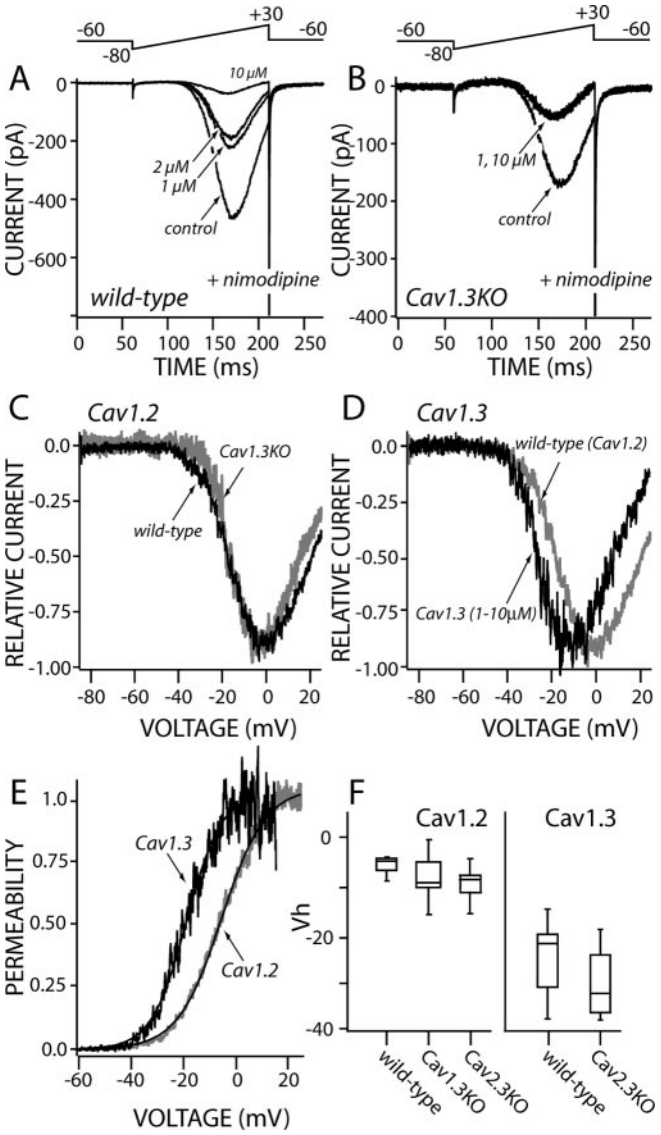

Figure 3. $Ca_V1.2$ and $Ca_V1.3$ channels differ in dihydropyridine sensitivity and voltage dependence. *A*, Ca^{2+} channel currents in wild-type medium spiny neurons show a high-affinity (<1 μM) and low-affinity (1–10 μM) block by nimodipine ($n = 5$). Neurons were recorded in the presence of ω-agatoxin TK (AgTx; 200 nM) and ω-conotoxin GVIA (CgTx; 1 μM) with Ba^{2+} (5 mM) as the charge carrier. Currents were elicited by a voltage protocol of −80 mV ramp to +30 mV (150 ms); the holding potential was −60 mV. *B*, Ca^{2+} channel currents in $Ca_V1.3$ knock-out medium spiny neurons show only the high-affinity block by nimodipine (1 μM; $n = 8$). Recording conditions were the same as for *A*. *C*, Currents blocked by 200 nM nimodipine from wild-type (black) and $Ca_V1.3$ knock-out neurons (gray) have similar voltage dependence. Conditions were as in *A* and *B*. *D*, Low-affinity channels (blocked by the increment from 1 to 10 μM nimodipine) in wild-type neurons (black) activated at more negative membrane potentials than currents blocked by 200 nM nimodipine (gray). *E*, Permeability estimates derived from the currents blocked by low (200 nM) and high (1–10 μM) nimodipine. Permeability estimates were fit with first-order Boltzmann functions: high-affinity $Ca_V1.2$, $V_h = -9$ mV; low-affinity $Ca_V1.3$, $V_h = -19$ mV. *F*, Statistical summary of half-activation voltages for high-affinity $Ca_V1.2$ currents (left) and low-affinity $Ca_V1.3$ currents (right). $Ca_V1.2$ currents blocked by 200 nM nimodipine: wild-type median, $V_h = -5$ mV ($n = 3$); $Ca_V1.3$ knock-out median, $V_h = -10$ mV ($n = 9$); $Ca_V2.3$ knock-out median, $V_h = -9$ mV ($n = 5$). Currents blocked by 10 μM but not 1 μM nimodipine: wild-type median, $V_h = -22$ mV ($n = 6$); $Ca_V2.3$ knock-out median, $V_h = -32$ mV ($n = 4$).

completely blocked by 1 μM nimodipine (Fig. 3*B*) ($n = 8$). These data show that medium spiny neurons coexpress $Ca_V1.2$ and $Ca_V1.3$ Ca^{2+} channels that can be separated primarily on the basis of their sensitivity to dihydropyridine antagonists. In addition, we studied the voltage dependence of the dihydropyridine block (Bean, 1984). $Ca_V1.2$ sensitivity was not affected by holding potential. In contrast, holding the membrane potential at −80 mV dramatically reduced $Ca_V1.3$ channel block by nimodipine, shifting the IC_{50} value by a factor of ~10 (Xu and Lipscombe, 2001).

This difference in nimodipine sensitivity was then used to determine whether $Ca_V1.2$ and $Ca_V1.3$ channels were biophysically distinguishable. To determine the voltage dependence of $Ca_V1.2$ channels, the currents that were resistant to blockade by 200 nM nimodipine were subtracted from control currents. This should yield currents that were solely attributable to $Ca_V1.2$ channels. $Ca_V1.2$ channel current–voltage plots derived from wild-type neurons peaked near 0 mV (Fig. 3*C*, black trace); currents isolated from $Ca_V1.3$ knock-out neurons were virtually identical (Fig. 3*C*, gray trace). $Ca_V1.3$ channel currents were operationally defined as those blocked by 10 μM but not 1 μM nimodipine. In contrast to $Ca_V1.2$ channels, these channels activated at relatively hyperpolarized membrane potentials (Fig. 3*D*). Permeability estimates were calculated to give a better picture of how channel open probability changed with voltage (Bargas et al., 1994). These estimates were readily fit with a single-site Boltzmann function (Fig. 3*E*). Based on this analysis, the half-activation voltage of $Ca_V1.3$ channels was ~15 mV more negative than that for $Ca_V1.2$ channels. The data from these experiments are summarized in a nonparametric format in Figure 3*F*. $Ca_V1.2$ channel currents had half-activation voltages of approximately −5 mV in wild-type neurons as well as in neurons from $Ca_V1.3$ and $Ca_V2.3$ knock-outs. In contrast, $Ca_V1.3$ channel currents had half-activation voltages between −20 and −25 mV in neurons from wild-type and $Ca_V2.3$ knock-out mice, significantly more negative than $Ca_V1.2$ channels ($n = 5$; $p < 0.05$, Mann–Whitney). These results show that medium spiny neurons coexpress functional $Ca_V1.2$ and $Ca_V1.3$ L-type channels and that these channels differ in both their dihydropyridine and voltage sensitivity. We next asked whether these two channels were differentially modulated by GPCRs.

D_2 dopaminergic and M_1 muscarinic receptors selectively modulate $Ca_V1.3$ channels

To determine whether $Ca_V1.2$ or $Ca_V1.3$ channels were targeted by D_2 receptor activation, recordings were made from medium spiny neurons in which the $Ca_V1.3$ subunit had been genetically deleted (Platzer et al., 2000). To our surprise, D_2 receptor agonists had no effect on tail currents in these neurons (Fig. 4*A*). This was not a consequence of D_2 receptor dysfunction, because the modulation of $Ca_V2.1/2.2$ channel currents evoked by the step depolarization, which relies on a distinct, membrane-delimited signaling cascade, remained. To verify that recordings were made from the subset of neurons expressing D_2 receptors, scRT-PCR profiling was performed. In a sample of six $Ca_V1.3$-deficient neurons expressing ENK mRNA, a reliable marker of D_2 receptor-expressing neurons (Gerfen, 1992; Surmeier et al., 1996), none exhibited a discernible reduction in tail amplitude after NPA application (Fig. 4*C*,*D*). In contrast, the modulation of the $Ca_V2.1/2.2$ (N, P/Q) currents evoked by the depolarizing step was not significantly altered ($n = 4$; median suppression control, 16%; $Ca_V1.3$ knock-out, 20%; $p > 0.05$, Kruskal–Wallis) (Hernandez-Lopez et al., 2000). To provide an additional test of the D_2 receptor selectivity, ramp currents in wild-type neurons were examined. Again, concentrations of nimodipine (1 μM) that fully block $Ca_V1.2$ channels failed to significantly reduce the effects of NPA, whereas concentrations of nimodipine (10 μM) that

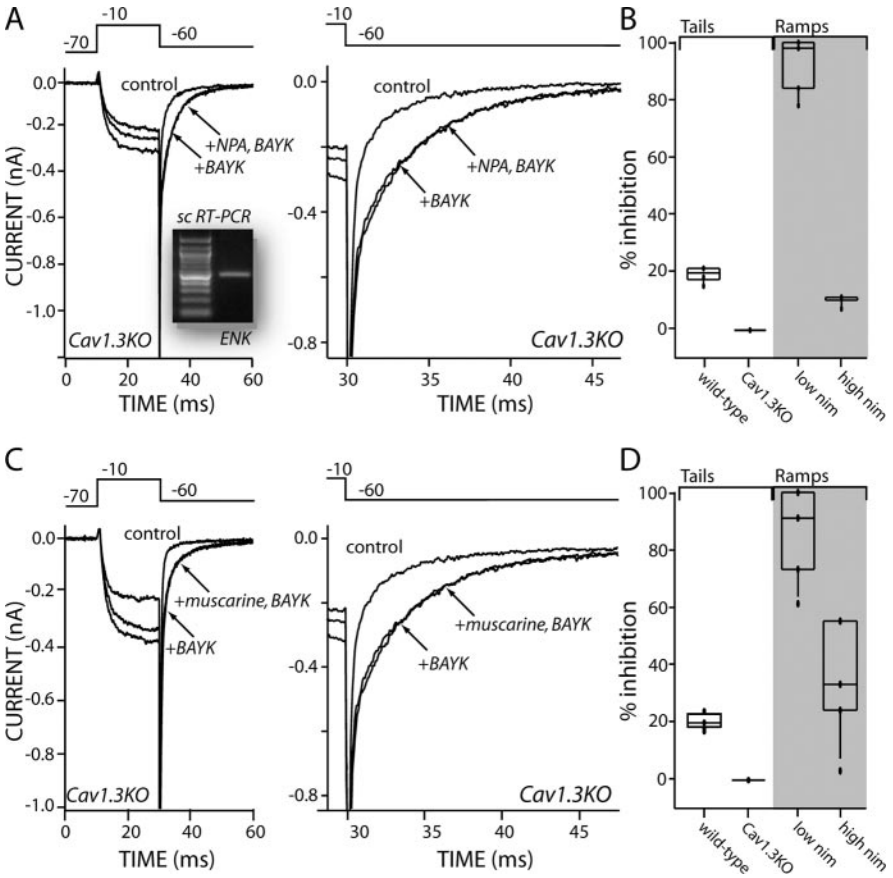

Figure 4. D_2 dopaminergic and M_1 muscarinic receptor modulations of L-type calcium channels is lost in neurons from a $Ca_V1.3$ knock-out. *A*, Current traces from a medium spiny neuron from a $Ca_V1.3$ knock-out mouse. Experimental conditions were the same as in Figure 1. NPA had no effect on the L-type tail current. The inset shows scRT-PCR confirmation that the neuron expressed enkephalin, a marker for D_2 receptor expression. *B*, Box plot illustrates the difference in percentage inhibition of L-type tail currents by D_2 receptor activation in medium spiny neurons from wild-type ($n = 3$; median, 18%) and $Ca_V1.3$ knock-out ($n = 6$; median, 0%) mice ($p < 0.05$; Mann–Whitney). Also shown is the box plot summary of experiments examining the reduction in peak ramp current by NPA (10 μM) after the addition of low (low nim; 1 μM; $n = 4$) and high (high nim; 10 μM; $n = 4$) nimodipine. The amplitude of the modulation in low and high nimodipine divided by the control modulation is plotted; values close to 100 indicate no effect on the modulation, whereas values close to 0 indicate occlusion. *C*, Current traces from a dorsal striatal medium spiny neuron from a $Ca_V1.3$ knock-out mouse. Experimental conditions were the same as Figure 1. Muscarine had no effect on the L-type tail current. *D*, Box plot illustrates the difference in percentage inhibition of L-type tail currents by M_1 receptor activation in medium spiny neurons from wild-type ($n = 5$; median, 20%) and $Ca_V1.3$ knock-out ($n = 5$; median, 0%) mice ($p < 0.05$; Mann–Whitney). Also shown is the box plot summary of experiments examining the reduction in peak ramp current by muscarine (10 μM) after the addition of low (low nim; 1 μM; $n = 5$) and high (high nim; 10 μM; $n = 5$) nimodipine. The amplitude of the modulation in low and high nimodipine divided by the control modulation is plotted; values close to 100 indicate no effect on the modulation, whereas values close to 0 indicate occlusion.

also blocked $Ca_V1.3$ channels occluded the modulation, leaving the residual $Ca_V2.1/2.2$ channel current modulation ($n = 4$) (Fig. 4*B*).

Next, the selectivity of M_1 muscarinic receptor linkage was examined. As with the D_2 receptor modulation, the effect of muscarine on the slow, L-type tail currents was abolished in neurons lacking $Ca_V1.3$ channels (Fig. 4*C*). This result suggests that activation of the ubiquitously expressed M_1 receptor, which is responsible for the suppression of L-type channel currents, selectively targets $Ca_V1.3$ channels. Despite the loss of this modulation, the M_4 muscarinic receptor suppression of $Ca_V2.1/2.2$ Ca^{2+} channels (Howe and Surmeier, 1995; Yan et al., 2001) was left intact in the $Ca_V1.3$-deficient neurons. This can be seen in the response to the step depolarization ($n = 5$; median suppression control, 19%; $Ca_V1.3$ knock-outs, 17%; $p > 0.05$, Kruskal–Wallis). To provide another test of the selectivity of the M_1 receptor modulation, ramp currents were recorded in wild-type neurons as described above. Concentrations of nimodipine (1 μM) that should fully block $Ca_V1.2$ channels failed to substantially alter the magnitude of the muscarinic modulation, whereas application of $Ca_V1.3$-inclusive concentrations of nimodipine (10 μM) occluded the effects of muscarine (Fig. 4*D*) ($n = 5$), leaving the residual M_4 modulation of $Ca_V2.1/2.2$ channels. Last, the voltage dependence of the current modulated by muscarine was estimated by subtracting the currents unaffected by muscarine from control currents. This analysis yielded currents with a half-activation voltage indistinguishable from that of $Ca_V1.3$ channels isolated pharmacologically ($n = 6$) (data not shown) (see supplemental figure, available at www.jneurosci.org as supplemental material).

Medium spiny neurons coexpress a long $Ca_V1.3$ channel splice variant and interacting Shank isoforms

Zhang et al. (2005) have shown that the scaffolding protein Shank selectively interacts with SH3 and PDZ binding domains in the C-terminal region of a long $Ca_V1.3$ splice variant ($Ca_V1.3a$). An interaction with Shank could bring $Ca_V1.3$ channels into physical proximity to D_2/M_1 receptors and elements of the signaling cascade they engage (Sheng and Kim, 2000). As a first step toward testing this hypothesis, whole striatal tissue was profiled for the presence of the two C-terminal splice variants of $Ca_V1.3$ expressed in the brain (Safa et al., 2001). Serial dilution RT-PCR revealed that both long ($Ca_V1.3a$) and short ($Ca_V1.3b$) variants were present but that $Ca_V1.3a$ was present at apparently higher levels (Fig. 5*A*). Profiling of individual medium spiny neurons confirmed this analysis, showing that $Ca_V1.3a$ mRNA was easily detected in both ENK- and SP-expressing subtypes of medium spiny neurons (14/15) (Fig. 5*B*). In contrast, $Ca_V1.3b$ was infrequently detected (2/15). This was not a limitation posed by the single-cell analysis, because $Ca_V1.3b$ was readily detected in dopaminergic neurons of the substantia nigra ($n = 5$) (Fig. 5*B*, right panel).

The C-terminal region of $Ca_V1.3a$ subunits binds preferentially with two of the three Shank isoforms found in the brain (Shank3/Shank1) (Zhang et al., 2005). If targeting of $Ca_V1.3$ channels was dependent on Shank in medium spiny neurons, they should express one or both of these isoforms. To determine whether this was the case, striatal tissue was assayed for Shank mRNA. At the tissue level, all three Shank isoforms were readily detected at nominally the same level of abundance (Fig. 5*C*). However, in medium spiny neurons, the Shank isoform with the highest affinity for the $Ca_V1.3a$ subunit, Shank3, appeared to be the most abundant, being detected in seven of eight cells. Shank1, which also has a high affinity for the $Ca_V1.3a$ terminal region, also

was readily detected (5/8), whereas Shank2 was not detected at all (0/8) (Fig. 5*D*). This pattern was cell-type specific, because examination of cholinergic interneurons failed to detect Shank2 or Shank3 but readily detected Shank1 (Fig. 5*E*) ($n = 6$).

Next, to determine whether $Ca_V1.3a$ channels and Shank were in close physical proximity, striatal tissue sections were studied using immunocytochemical approaches. Because both $Ca_V1.3a$ and Shank antibodies were raised in the same host, colabeling of the same section was not possible. Because PSD-95 is colocalized with Shank at excitatory synapses (Sheng and Kim, 2000), it was used as a surrogate marker. As expected, PSD-95 immunoreactivity in striatal tissue had a punctate distribution (Fig. 6*A*, top left), reflecting the localization of excitatory synapses predominantly on dendritic spine heads (Kennedy, 1998; Bolam et al., 2000). Shank immunoreactivity was punctate as well but had an additional somatic component that presumably reflected cytoplasmic protein (Fig. 6*A*, top center). Color overlays from 500 nm optical sections provided evidence that these two proteins had a significant level of colocalization (Fig. 6*A*, top right). However, the images were not perfectly aligned, as one might expect if the proteins were slightly displaced from one another near synapses. To quantify the relationship, spatial cross-correlations were computed on aligned image fields after standardizing the optical image intensity (Li et al., 2004). To reduce spurious correlations attributable to somatic labeling, fields in which there were few visible somata were chosen for analysis. This analysis consistently revealed a strong spatial correlation between PSD-95 and Shank labeling that was strongest with no image displacement and then sharply declined within $\sim 1\ \mu m$, approximately the dimension of a spine (Fig. 6*B*). In a sample of five sections, the median peak cross-correlation was 0.35 (range, 0.71–0.23). The secondary slower decline in the cross-correlation in Figure 6*B* reflected somatic labeling, because it was absent in correlations from subfields lacking any obvious somatic profiles.

$Ca_V1.3a$ immunolabeling was strikingly similar to that for PSD-95, being distinctly punctate (Fig. 6*A*, bottom center). Overlays of regions processed for both PSD-95 and $Ca_V1.3a$ revealed a significant degree of colocalization (Fig. 6*A*, bottom right). To quantify the relationship between the two markers, cross-correlation analysis was performed as for Shank and PSD-95. Analysis of five different sections consistently found a strong relationship between PSD-95 and $Ca_V1.3$ labeling with peak values between 0.28 and 0.41 (Fig. 6*C*) ($n = 5$). As with Shank, the peak cross-correlation was found near zero displacement and then fell rapidly to baseline within the expected dimensions of a spine. These data suggest that PSD-95, Shank, and $Ca_V1.3a$ subunits are colocalized in medium spiny neurons at excitatory synapses, which are predominantly found on spines.

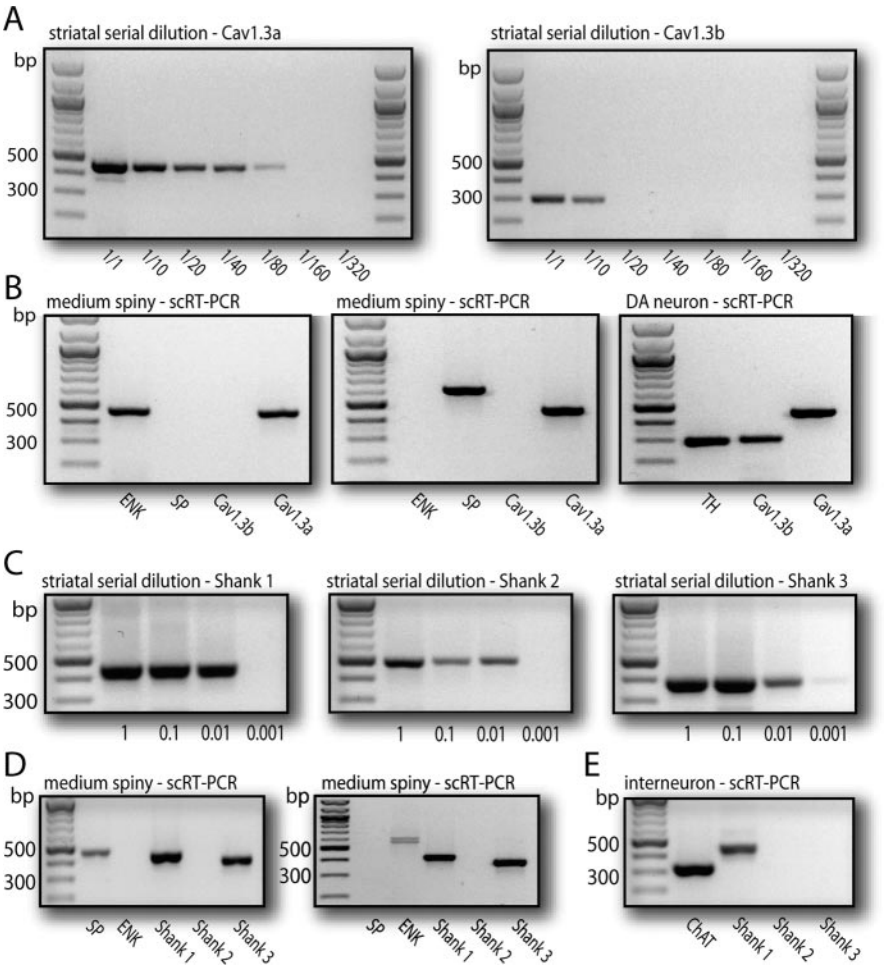

Figure 5. Medium spiny neurons primarily express $Ca_V1.3a$ and Shank1 and Shank3 mRNAs. *A*, Serial dilutions of amplified cDNA from whole-tissue dorsal striatum illustrate that both $Ca_V1.3$ short ($Ca_V1.3b$) and long ($Ca_V1.3a$) forms were present in the dorsal striatum, but $Ca_V1.3$ long form was detected at a higher frequency. *B*, Single-cell RT-PCR from a striatal medium spiny neuron shows that $Ca_V1.3a$ mRNA was detected in both ENK- and SP-expressing medium spiny neurons. In dopaminergic neurons, both $Ca_V1.3a$ and $Ca_V1.3b$ mRNA were readily detected (right). *C*, Serial dilutions of amplified cDNA from whole-tissue dorsal striatum illustrate that Shank1 and Shank3 were detected at higher levels compared with Shank2, as shown by the robust signal. *D*, Single-cell RT-PCR from a striatal medium spiny neuron shows that Shank1 and Shank3 mRNA were readily detected. *E*, In a cholinergic interneuron, Shank1 but not Shank3 mRNA was detected.

PSD-95, Shank, and $Ca_V1.3a$ channels appear to be in close physical proximity in medium spiny neurons, but are they bound to one another? To test this possibility, coimmunoprecipitation experiments were performed. Extracts of rat brain synaptosomes were prepared, and protein was immunoprecipitated using an anti-$Ca_V1.3a$ rabbit pAb. A Western blot of this protein was then probed with guinea pig anti-Shank pAb, revealing Shank (Fig. 6*D*). Shank immunoreactivity was lost by preincubation with $Ca_V1.3a$ C-terminal peptide, demonstrating the specificity of the precipitation.

Dialysis with a peptide mime of the $Ca_V1.3a$ PDZ binding domain disrupts the D_2 and M_1 receptor modulation

If the interaction between Shank and $Ca_V1.3a$ subunits is critical to the selective modulation by D_2 and M_1 receptors, competitive inhibitors of this binding should disrupt the modulation. Zhang et al. (2005) have shown that Shank1/3 binds to a $Ca_V1.3a$ "ITTL" PDZ motif but does not bind strongly to a $Ca_V1.2$ "VSNL" PDZ motif. Therefore, peptides containing the ITTL motif should act as efficient competitive inhibitors of the Shank-$Ca_V1.3a$ interaction, whereas peptides containing the VSNL motifs should not.

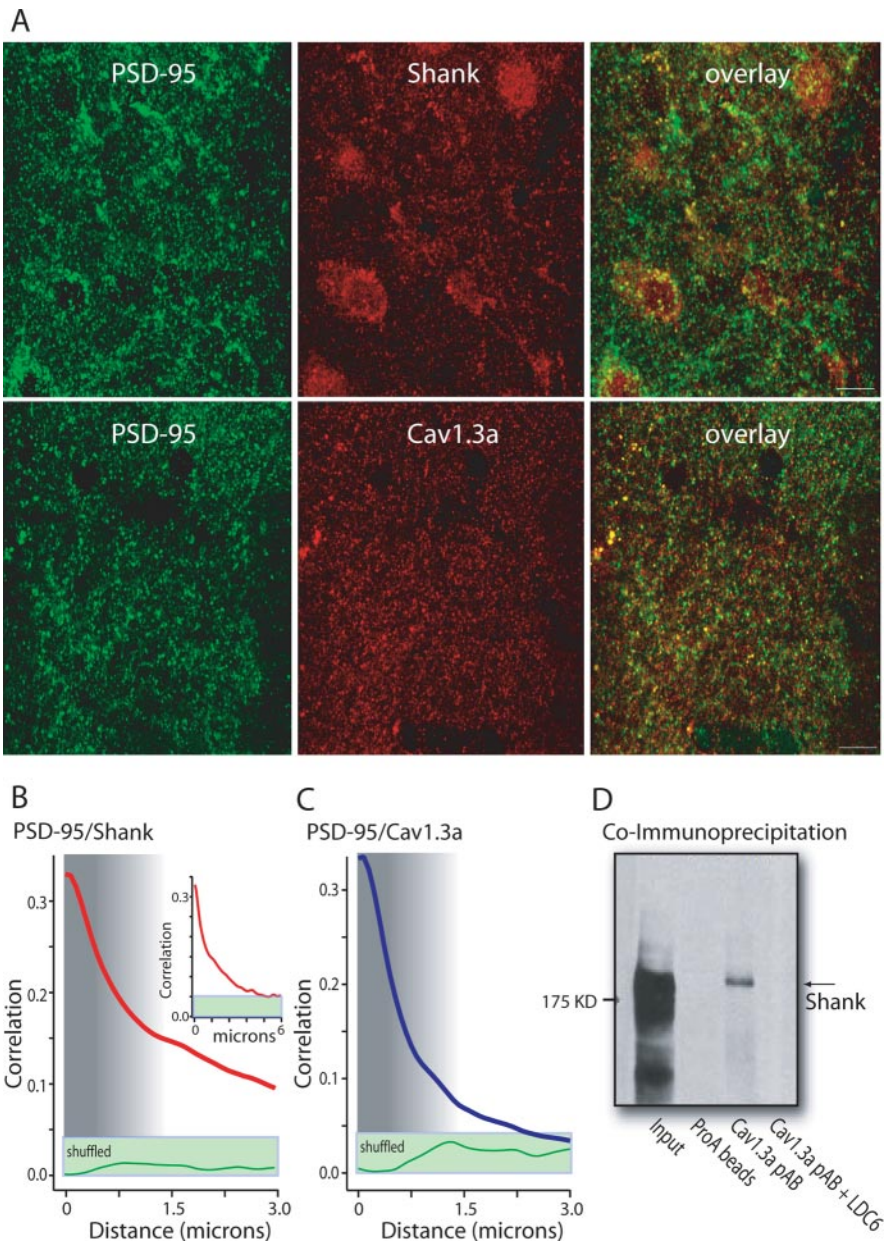

Figure 6. PSD-95, Shank and $Ca_V1.3a$ proteins colocalize in striatal tissue. *A*, Top row, Confocal images of striatal tissue sections processed for PSD-95 (green) and Shank (red). Overlays of the images revealed a significant level of colocalization that appears yellow. Bottom row, Different striatal section processed for PSD-95 (green) and $Ca_V1.3a$ (red). Both labels have a punctate distribution. Overlaying the images at the right revealed a significant level of colocalization as judged by the appearance of yellow puncta. *B*, Spatial cross-correlation between PSD-95 and Shank computed from the image shown in the top row of *A*. The inset is the correlation run out to 6 μm showing that the correlation drops to insignificant levels at this distance. The shuffled trace was obtained by randomly shifting the rows and columns of the Shank image and then recomputing the cross-correlation. *C*, Spatial cross-correlation of PSD-95 and $Ca_V1.3a$ images shown at the bottom of *A*. Note the strong correlation that rapidly falls within ~1.5 μm. Again, the shuffled cross-correlation was obtained by randomly shifting the rows and columns of the $Ca_V1.3a$ image and recomputing the correlation. *D*, Lysates from P2 rat brain synaptosomes were immunoprecipitated with anti-$Ca_V1.3a$ pAb (AM9742) and analyzed by Western blotting with anti-Shank guinea pig pAb (EK1123). The input lane contains one-fiftieth of synaptosomal lysate used for immunoprecipitation experiments. LDC6 peptide (2132–2155 of rat $Ca_V1.3a$) was added to the immunoprecipitation reactions as indicated at 400 μg/ml concentration.

To provide a functional test of this hypothesis, we turned back to acutely isolated medium spiny neurons in which the modulation of L-type Ca^{2+} channels could be examined. Although this preparation affords excellent experimental control, the principle regions of excitatory synaptic contact are removed, eliminating much of the structure hypothetically responsible for the selective modulation of $Ca_V1.3a$ channels. To determine whether some of this organization remained after dissociation, neurons were probed with Shank and $Ca_V1.3$ antibodies. As shown in Figure 7*A*, despite the dendritic truncation, punctate labeling for Shank and $Ca_V1.3a$ protein was found in the proximal dendrites of dissociated neurons. It is worth noting that D_2 or M_1 receptor agonists failed to modulate L-type currents in neurons lacking any visible dendrite ($n > 20$).

Having demonstrated that a portion of the scaffolding remained in the dissociated neurons, peptide mimes of the PDZ binding domains were introduced through the patch pipette during whole-cell recordings. The ability of D_2 receptor agonists to modulate L-type Ca^{2+} channel currents was unaffected by dialysis with the VSNL peptide but was disrupted by dialysis with an ITTL peptide (Fig. 7*C–E*). The modulation of the step currents, which was mostly attributable to $Ca_V2.1/2.2$ channel currents, was not significantly altered by either peptide, arguing that the receptor signaling mechanisms were intact [median control suppression, 16% ($n = 4$); +VSNL, 21% ($n = 4$); +ITTL, 10% ($n = 5$); $p > 0.05$, Kruskal–Wallis]. Similarly, M_1 receptor modulation of L-type Ca^{2+} channel currents was not affected by dialysis with the VSNL peptide (Fig. 7*F,H*) ($n = 4$). In contrast, dialysis with an ITTL peptide dramatically reduced the ability of M_1 receptors to modulate L-type currents (Fig. 7*G,H*) ($n = 5$; $p < 0.05$, Mann–Whitney). As with the dopaminergic modulation, the modulation of the currents evoked by the step, which were attributable to primarily the M_4 receptor modulation of $Ca_V2.1/2.2$ Ca^{2+} channels, was not significantly affected by the VSNL or ITTL peptides [median control suppression, 19% ($n = 5$); +VSNL, 21% ($n = 5$); +ITTL, 10% ($n = 5$); $p > 0.05$, Kruskal–Wallis]. Moreover, neither ITTL ($n = 8$) nor VSNL ($n = 4$) peptide had any significant effect on current density or voltage dependence (data not shown) ($n = 5$; $p > 0.05$, Kruskal–Wallis). The failure of the VSNL peptide to alter the D_2 and M_1 receptor modulations of tail currents was not a consequence of its inability to compete for the $Ca_V1.2$ PDZ domain, because dialysis of the peptide into cortical pyramidal neurons effectively blocked the 5-HT_2 receptor modulation of $Ca_V1.2$ channel currents ($n = 5$; control suppression, 26%; +VSNL, 10%; $p < 0.05$, Kruskal–Wallis) (Day et al., 2002).

The data presented thus far suggest that the ability of D_2 and M_1 receptors to suppress $Ca_V1.3$ Ca^{2+} channel currents depends on channel binding of Shank3/Shank1 proteins. However, why is this interaction important? Our previous studies have shown that the modulation of L-type channels depends on mobilization of

Ca^{2+} from IP_3R-controlled intracellular stores (Howe and Surmeier, 1995; Hernandez-Lopez et al., 2000). Shank may serve to bring $Ca_V1.3a$ channels close to IP_3Rs and these release sites. One way in which this could be accomplished is through Homer adaptor proteins, which are known to bind to both IP_3Rs and Shank through Ena/VASP homology 1 (EVH1) domains (Xiao et al., 2000). If this were the case, medium spiny neurons should express Homer isoforms possessing coiled-coil (CC) regions (Homer 1b-d, Homer 2–3) that allow self-association and assembly of the Shank-Homer-IP_3R scaffold. Indeed, in agreement with the predictions of *in situ* hybridization work (Shiraishi et al., 2004), scRT-PCR profiling of the GABAergic medium spiny neurons ($n = 17$) revealed expression of Homer 1b/c (16/17), Homer 1d (12/17), and Homer 2 (11/17) but lower levels of the Homer splice variant lacking these domains (Homer1a, 9/17) and Homer 3 (0/17) (Fig. 8*A*). To provide a functional test for the involvement of Homer proteins, neurons were dialyzed with a peptide targeting the EVH domain that should competitively inhibit Shank and IP_3R binding. Doing so suppressed the M_1 receptor modulation of $Ca_V1.3$ channel currents ($n = 6$), but dialysis of a similar peptide lacking the EVH binding domain (HBP-KE) failed to alter the modulation ($n = 3$) (Fig. 8*B*). These data are consistent with the hypothesis that Homer proteins are part of the Shank scaffold necessary for selective modulation of $Ca_V1.3$ channels.

D_2 receptor suppression of $Ca_V1.3$ Ca^{2+} channel currents dramatically reduce upstate transitions

Shank is thought to act as a scaffold at glutamatergic synapses (Sheng, 2001). In medium spiny neurons, the principal glutamatergic input arises from corticostriatal axons that terminate on dendritic spines (Bolam et al., 2000). *In vivo*, convergent activation of this input induces depolarized episodes called upstate, during which neurons can spike (Wilson, 1993). Recently, an *in vitro* slice model of these state transitions has been described that utilizes repetitive cortical stimulation or low micromolar concentrations of NMDA that induce tonic firing in corticostriatal pyramidal neurons (Vergara et al., 2003). In this model, upstates are dependent not only on synaptic input but postsynaptic L-type channels that help create dendritic plateau potentials, maintaining the upstate. Positioning of low-threshold $Ca_V1.3a$ channels at dendritic spines would be one way in which this

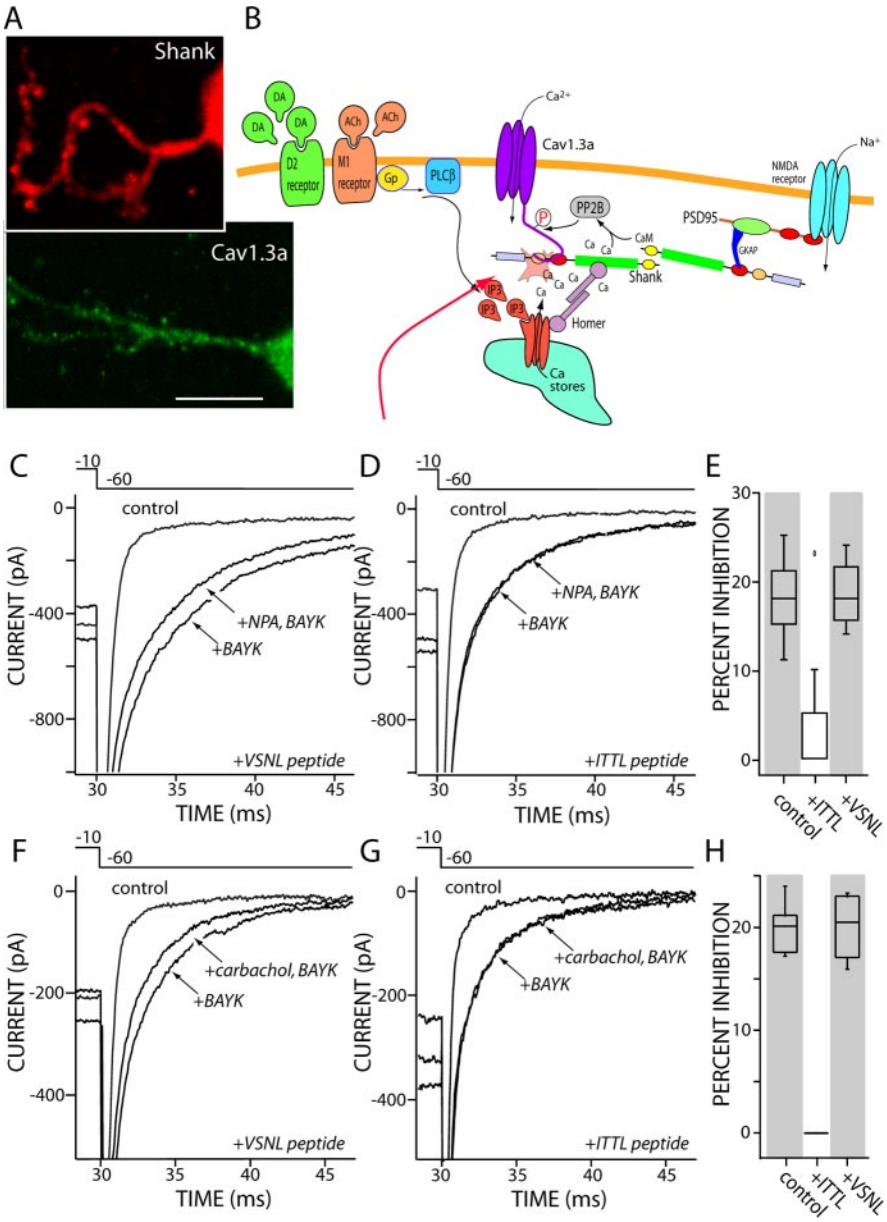

Figure 7. Peptides targeting the Shank PDZ domain disrupts D_2 and M_1 receptor modulation of $Ca_V1.3$ channels. *A*, Photomicrograph of acutely isolated medium spiny neurons showing punctate labeling for Shank (red) and $Ca_V1.3a$ (green), indicating that the isolation left a portion of the scaffolding intact. *B*, Schematic showing the hypothesized scaffolding complex at synaptic sites. Also shown is the site of the ITTL peptide targeting the Shank PDZ binding domain interacting with $Ca_V1.3a$. DA, Dopamine; ACh, acetylcholine; Gp, G-protein; Homer, protein homologous to Ena/vasodilator-stimulated phosphoprotein and Wiskott-Aldrich syndrome protein; Shank, SH3 domain and ankyrin repeat containing protein; CaM, calmodulin; GKAP, guanylate kinase associated protein; PP2B, protein phosphatase 2B/calcineurin (Sheng and Kim, 2000; Xiao et al., 2000). *C*, Modulation of tail currents by application of NPA (10 μM) in a neuron dialyzed with $Ca_V1.2$ VSNL peptide for 5 min. *D*, Tail currents in a wild-type medium spiny neuron after dialysis with the ITTL peptide for 5 min. Note the lack of tail modulation, yet the step current modulation mediated by D_2 receptors was normal. *E*, Box plot summarizes the results obtained from a sample of seven neurons with the ITTL peptide and four neurons with the VSNL peptide. The difference between the two treatment conditions was statistically significant ($p < 0.05$; Mann–Whitney). *F*, M_1 receptor modulation of tail currents in a wild-type medium spiny neuron after dialysis with the $Ca_V1.2$ VSNL peptide for 5 min. The recording conditions are the same as in previous figures except that the muscarinic receptor agonist carbamylcholine chloride (carbachol; 10 μM) was used (medium spiny neurons do not express nicotinic receptors; the addition of mecamylamine had no effect on the response). Similar results were obtained with muscarine. *G*, After dialysis for 5 min with the ITTL peptide, the M_1 receptor modulation of the tail currents is lost, but the M_4 receptor modulation of the step currents is retained. *H*, Box plot summarizes the results obtained from a sample of five neurons with the ITTL peptide and four neurons with the VSNL peptide. The differences between the two treatment conditions were statistically significant ($p < 0.05$; Mann–Whitney).

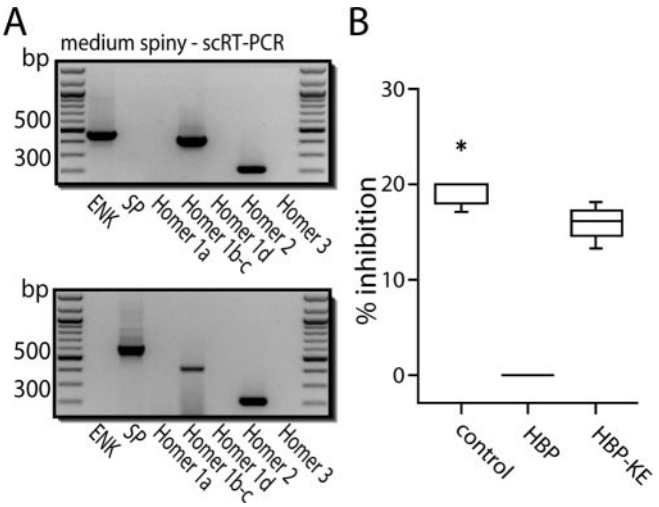

Figure 8. Homer mRNA is expressed in medium spiny neurons, and binding of Homer is necessary for M_1 muscarinic receptor modulation of $Ca_V1.3$ L-type calcium channels. *A*, Single-cell RT-PCR from a striatal medium spiny neuron shows that Homer 1b/c and Homer 2 are readily detected in both ENK- and SP-expressing medium spiny neurons. *B*, Carbachol application (10 μl) had no effect on L-current in medium spiny neurons dialyzed with Homer binding protein (HBP) (median, 0%; $n = 6$). In medium spiny neurons dialyzed with HBP-KE control peptide, L-current was inhibited by carbachol (median, 16%; $n = 3$; $p < 0.05$, Mann–Whitney). Also shown is the muscarine inhibition of medium spiny neurons from wild-type mice (median, 20%; $n = 5$). There is no difference between the control group of neurons without peptide dialysis and the group of neurons dialyzed with HBP-KE ($p > 0.05$; Mann–Whitney). The asterisk is an "outlier," a point that is >1.5 times the interquartile range beyond the interquartiles in the box plot (Tukey, 1977; Song et al., 2000).

glutamatergic receptor driven dendritic electrogenesis could occur. To test for the involvement of $Ca_V1.3$ channels in this phenomenon, upstates were examined in neurons recorded in slices from wild-type and $Ca_V1.3$ knock-out mice. Because medium spiny neurons express very low or undetectable levels of $Ca_V1.3b$ mRNA (see above), the deletion of the $Ca_V1.3$ gene should mimic the selective deletion of $Ca_V1.3a$ subunits. In wild-type neurons, spontaneous upstates were seen in most of the neurons (7 of 10) recorded after bath application of NMDA (5 μM) (Fig. 9*A*). In contrast, upstates were not seen in neurons from the $Ca_V1.3$ knock-out under identical recording conditions ($n = 5$) (Fig. 9*B*). This deficit did not appear to arise from an alteration in synaptic function, because local electrical stimulation evoked robust glutamatergic EPSPs, and miniature EPSPs were, if anything, elevated in frequency in $Ca_V1.3$-deficient neurons (data not shown). Additional evidence that these neurons were otherwise viable came from experiments where bath application of BayK 8644 (1 μM) enabled occasional upstate transitions in these neurons ($n = 3$), presumably by shifting the voltage dependence of the remaining $Ca_V1.2$ channels into the range of normal $Ca_V1.3$ channel gating (Bargas et al., 1994) (Fig. 9*B*, inset).

To determine whether GPCR suppression of $Ca_V1.3$ channels could transiently suppress upstate generation, medium spiny neurons were recorded as described above, and the D_2 agonist NPA was applied locally through a puffer pipette. M_1 receptor agonists were not examined because they also modulate K^+ channels involved in state transitions (W. Shen and Surmeier, unpublished observations). Before NPA application, in the presence of NMDA (5 μM), neurons spontaneously oscillated between upstates and downstates, yielding a distinctly bimodal membrane potential distribution ($n = 6$) (Fig. 9*C*,*D*). In four of six neurons, the application of NPA (10 μM) reversibly suppressed the generation of upstates causing the membrane potential distribution to become unimodal (Fig. 9*C*,*D*); in the other two neurons, NPA had no discernible effect. Although there are undoubtedly other ion channels participating in the state transitions that are potentially targets of modulation, these data are consistent with the hypothesis that modulation of synaptically located $Ca_V1.3a$ channels is an important component of the cellular response to D_2 receptor activation.

Discussion

M_1 and D_2 receptor signaling cascades selectively modulate $Ca_V1.3$ L-type Ca^{2+} channels

Previous studies have shown that D_2 dopaminergic and M_1 muscarinic receptors suppress L-type Ca^{2+} currents in striatal medium spiny neurons (Howe and Surmeier, 1995; Hernandez-Lopez et al., 2000). Although robust, the suppression of L-type Ca^{2+} currents by these GPCR cascades is invariably incomplete, suggesting that some channels are targeted for modulation and others are not. This differential vulnerability appears to turn in large measure on molecular heterogeneity of the L-type channels themselves. Medium spiny neurons express two major classes of L-type Ca^{2+} channels: one possessing a pore-forming $Ca_V1.2$ subunit and the other with a $Ca_V1.3$ subunit. Four lines of evidence support this conclusion. First, scRT-PCR profiling revealed that both major classes of medium spiny neurons coexpress $Ca_V1.2$ and $Ca_V1.3$ subunit mRNAs. Second, L-type Ca^{2+} channels in medium spiny neurons were heterogeneous in their affinity for dihydropyridines; one component was blocked with high affinity by the dihydropyridine L-type channel antagonist nimodipine (IC_{50}, ~200 nM), whereas another component was blocked only at higher antagonist concentrations (IC_{50}, ~2 μM). This affinity difference is just what is expected of $Ca_V1.2$ and $Ca_V1.3$ channels from work in heterologous expression systems (Safa et al., 2001; Xu and Lipscombe, 2001). More compelling perhaps was the loss of the lower affinity component in neurons from $Ca_V1.3$ knock-out mice and its preservation in $Ca_V2.3$ knock-outs. Third, as in heterologous expression systems (Xu and Lipscombe, 2001), Ca^{2+} channels with a low dihydropyridine affinity ($Ca_V1.3$) opened at more negative membrane potentials than did high affinity $Ca_V1.2$ channels. Nominal $Ca_V1.3$ channel half-activation voltages were 10–15 mV more negative than those for $Ca_V1.2$ channels. Fourth, immunocytochemical analysis revealed the presence of $Ca_V1.3$ protein in medium spiny neurons, complementing previous work showing $Ca_V1.2$ expression (Hell et al., 1993b).

Three lines of evidence argue that D_2 and M_1 receptor signaling cascades differentially regulate these two channel types. The first comes from the failure of either GPCR to modulate BayK 8644 tail currents in neurons where functional $Ca_V1.3$ subunits had been genetically deleted. The second comes from the ability of high, but not low, $Ca_V1.2$-selective concentrations of dihydropyridine antagonists to occlude the modulation. The third comes from the similarity in gating voltage dependence of the modulated channels and $Ca_V1.3$ Ca^{2+} channels.

The selective modulation appears to be dependent on Shank3/Shank1 binding to $Ca_V1.3a$ subunits

One way in which this kind of signaling specificity could be achieved is by bringing the receptors, channels, and signaling elements to the same subcellular locale. The best-characterized signaling complex of this sort is the postsynaptic density at glutamatergic synapses, where scaffolding or anchoring proteins organize and concentrate transduction proteins (Kennedy, 1998; Sheng and Kim, 2000). Shank has been referred to as a "master"

scaffolding protein at these sites because of its prominence and capacity to link a broad array of participating proteins. Zhang et al. (2005) have expanded this list to include L-type Ca^{2+} channels containing $Ca_V1.3$ subunits, showing that Shank proteins selectively bind to a long C-terminal splice variant of this subunit via SH3 and PDZ domains. This interaction promotes synaptic targeting of the channel in hippocampal neurons.

Targeting of this type also appears to occur in striatal medium spiny neurons. In addition to the long splice variant of the $Ca_V1.3$ subunit ($Ca_V1.3a$), these neurons expressed mRNA for interacting Shank isoforms (Shank3, Shank1). Confocal analysis of immunocytochemical labeling showed that $Ca_V1.3a$ and Shank proteins colocalized with the synaptic protein PSD-95 within a spatial domain expected of a spine, the predominant site of glutamatergic synapses in medium spiny neurons (Bolam et al., 2000; Sheng, 2001). A direct physical interaction was supported by the coimmunoprecipitation of $Ca_V1.3a$ and Shank proteins. Moreover, recent Ca^{2+} imaging studies have shown that L-type channels contribute to intraspine Ca^{2+} dynamics in medium spiny neurons (Carter and Sabatini, 2004), complementing work showing a similar localization elsewhere (Simon et al., 2003; Hoogland and Saggau, 2004).

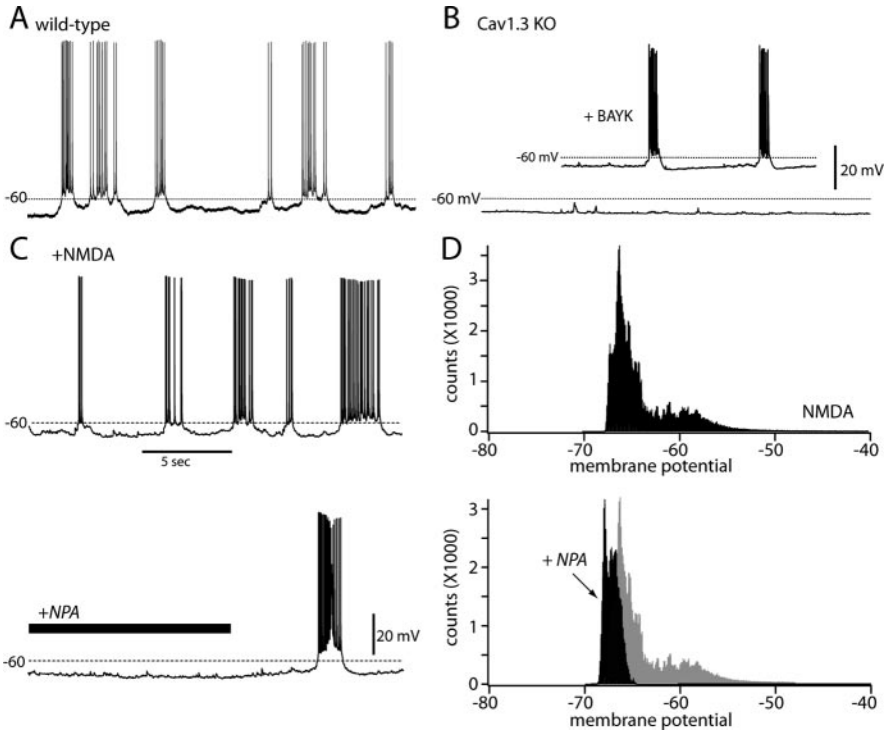

Figure 9. D_2 receptor modulation of $Ca_V1.3$ channel currents suppresses upstate generation in response to glutamatergic receptor stimulation in striatal medium spiny neurons. *A*, Upstate transitions in a striatal medium spiny neuron recorded in a tissue slice from a wild-type mouse. *B*, In the same condition, medium spiny neurons in a slice from a $Ca_V1.3$ null mouse failed to exhibit upstate transitions, unless the L-type channel agonist BayK 8644 (1 μM) was added to the bath. This agonist shifts the voltage dependence of $Ca_V1.2$ L-type channel activation, making them resemble $Ca_V1.3$ channels. *C*, Upstate transitions in a medium spiny neuron recorded in a slice preparation before and after application of the D_2 receptor agonist NPA (10 μM). *D*, All-points histogram showing the bimodal membrane potential distribution before NPA application and the unimodal distribution after D_2 receptor activation.

The functional association between Shank and $Ca_V1.3a$ Ca^{2+} channels also appears to be necessary for GPCR regulation. Dialysis with a competitive inhibitor of the $Ca_V1.3a$-Shank PDZ domain (ITTL) dramatically attenuated the ability of D_2 and M_1 GPCRs to suppress $Ca_V1.3$ L-type currents, whereas dialysis with a competitive inhibitor of the $Ca_V1.2$ PDZ binding domain (VSNL) was without effect on the modulation. Because PDZ domains are commonly used to link proteins in neurons, it is possible that effect of the ITTL peptide is attributable to disruption of some other PDZ-dependent, protein–protein interaction. However, the failure of the closely related VSNL PDZ peptide to attenuate the $Ca_V1.3$ channel modulation argues against this possibility, especially in light of the ability of this construct to disrupt the modulation of $Ca_V1.2$ channels in cortical pyramidal neurons. Nevertheless, additional study on this point is warranted.

Additional evidence for the importance of Shank in the regulation of $Ca_V1.3$ channels comes from the ability of peptides targeting the EVH1 binding site of Homer to attenuate GPCR effects. This site enables Homer isoforms to bind to the proline-rich region of Shank (Sheng and Kim, 2000). Dimerization of Homer isoforms having CC domains creates a way in which IP_3-regulated intracellular Ca^{2+} stores could be brought into close physical proximity to Shank and $Ca_V1.3$ channels (Xiao et al., 2000). Previous studies have strongly implicated these stores in both D_2 and M_1 receptor modulations of L-type channels (Howe and Surmeier, 1995; Hernandez-Lopez et al., 2000). Because Ca^{2+} is rapidly buffered in dendrites (Sabatini et al., 2002), bringing the IP_3R release sites close to the channels could be critical to the efficient activation of the remaining elements in the Ca^{2+}-dependent modulatory cascade. Calcineurin, which is thought to be the final effector of the D_2/M_1 receptor cascade, is anchored by A-kinase anchoring protein 79/150, a known participant in PSD-95 scaffolds (Altier et al., 2002; Gomez et al., 2002). The recent discovery of that calcineurin-mediated modulation of $Ca_V1.3$ channels is controlled by the calmodulin binding phosphoprotein regulator of calcium/calmodulin-dependent signaling (Rakhilin et al., 2004) creates a rich intraspine regulatory network. Although GPCR positioning is less well characterized, there is growing evidence that they also can interact with synaptic scaffolding proteins (Davare et al., 2001; Kreienkamp, 2002). Such an interaction is consistent with ultrastructural studies showing that both D_2 and M_1 receptors are enriched at synaptic sites in medium spiny neurons (Hersch et al., 1994, 1995; Bolam et al., 2000).

This picture complements the growing recognition that $Ca_V1.2$ channels also participate in neuronal synaptic signaling complexes. In hippocampal pyramidal neurons, $\beta 2$ adrenergic receptors assemble with $Ca_V1.2$ channels, protein kinase A, protein phosphatase 2A, and adenylyl cyclase in perisomatic and dendritic sites (Davare et al., 2001). Although the mechanism remains to be determined, this close association enables $\beta 2$ receptor agonists to rapidly enhance $Ca_V1.2$ channel currents in a spatially restricted manner. Scaffolding that is dependent on neuronal interleukin-16 PDZ domains could be a factor in the GPCR association, as it is in $Ca_V1.2$ channel-dependent CREB phosphorylation (Weick et al., 2003). Given their biophysical differ-

ences, it is tempting to speculate that coexpression of $Ca_V1.2$ and $Ca_V1.3$ channels enables neurons to sense and signal over a much broader activity range than would be possible with either channel alone.

GPCR-Shank-$Ca_V1.3$ channel complex regulates glutamatergic receptor driven upstates in medium spiny neurons

The recruitment of $Ca_V1.3$ channels to synaptic signaling complexes by Shank proteins provides a framework in which we can begin to understand activity-dependent plasticity in medium spiny neurons. *In vivo*, glutamatergic synaptic input promotes the transition from a hyperpolarized downstate to a depolarized upstate (Wilson, 1993). Although the upstate transitions depend on glutamatergic receptors for their initiation, postsynaptic voltage-dependent ion channels clearly shape their duration and potential envelope. L-type channels appear to be particularly important in this phenomena, because dihydropyridine antagonists suppress upstate transitions and agonists promote them (Vergara et al., 2003). Our data extend these findings by showing the loss of upstate transitions in neurons from $Ca_V1.3$ knock-out mice or in neurons after activation of GPCRs that suppress $Ca_V1.3$ channel currents. This disruption suggests that there is a synergy between glutamatergic receptors and $Ca_V1.3$ channels in the generation of upstates that is regulated by D_2 dopaminergic receptors.

The strategic positioning of $Ca_V1.3$ channels afforded by Shank also may be a critical factor in determining how afferent synaptic activity is translated into long-term alterations in neuronal function. For example, in striatal neurons, long-term synaptic depression (LTD) is dependent on opening of L-type Ca^{2+} channels (Calabresi et al., 1994). Synaptic scaffolding of $Ca_V1.3$ channels may be critical to LTD induction. Activity-dependent alterations in the phosphorylation state of transcription factors that signal synaptic events to the nucleus may also be depend on "privileged positioning" of L-type Ca^{2+} channels (Cepeda et al., 1998; Rajadhyaksha et al., 1999; Zhang et al., 2005). The inclusion of D_2 and M_1 GPCRs in this synaptic complex creates a mechanism by which the two most clinically important striatal modulators (dopamine and acetylcholine) could regulate this plasticity.

References

Albin RL, Young AB, Penney JB (1989) The functional anatomy of basal ganglia disorders. Trends Neurosci 12:366–375.

Altier C, Dubel SJ, Barrere C, Jarvis SE, Stotz SC, Spaetgens RL, Scott JD, Cornet V, De Waard M, Zamponi GW, Nargeot J, Bourinet E (2002) Trafficking of L-type calcium channels mediated by the postsynaptic scaffolding protein AKAP79. J Biol Chem 277:33598–33603.

Avery RB, Johnston D (1996) Multiple channel types contribute to the low-voltage-activated calcium current in hippocampal CA3 pyramidal neurons. J Neurosci 16:5567–5582.

Bading H, Ginty DD, Greenberg ME (1993) Regulation of gene expression in hippocampal neurons by distinct calcium signaling pathways. Science 260:181–186.

Bargas J, Howe A, Eberwine J, Cao Y, Surmeier DJ (1994) Cellular and molecular characterization of Ca^{2+} currents in acutely isolated, adult rat neostriatal neurons. J Neurosci 14:6667–6686.

Bean BP (1984) Nitrendipine block of cardiac calcium channels: high-affinity binding to the inactivated state. Proc Natl Acad Sci USA 81:6388–6392.

Bendat J, Piersol A (1971) Random data: analysis and measurement procedures, pp 28–31. New York: Wiley.

Bernard V, Normand E, Bloch B (1992) Phenotypical characterization of the rat striatal neurons expressing muscarinic receptor genes. J Neurosci 12:3591–3600.

Bolam JP, Hanley JJ, Booth PA, Bevan MD (2000) Synaptic organisation of the basal ganglia. J Anat 196:527–542.

Bolshakov VY, Siegelbaum SA (1994) Postsynaptic induction and presynaptic expression of hippocampal long-term depression. Science 264:1148–1152.

Bowden SE, Fletcher S, Loane DJ, Marrion NV (2001) Somatic colocalization of rat SK1 and D class (Ca(v)1.2) L-type calcium channels in rat CA1 hippocampal pyramidal neurons. J Neurosci 21:RC175.

Calabresi P, Pisani A, Mercuri NB, Bernardi G (1994) Post-receptor mechanisms underlying striatal long-term depression. J Neurosci 14:4871–4881.

Carter AG, Sabatini BL (2004) State-dependent calcium signaling in dendritic spines of striatal medium spiny neurons. Neuron 44:483–493.

Catterall WA (1998) Structure and function of neuronal Ca^{2+} channels and their role in neurotransmitter release. Cell Calcium 24:307–323.

Cepeda C, Colwell CS, Itri JN, Chandler SH, Levine MS (1998) Dopaminergic modulation of NMDA-induced whole cell currents in neostriatal neurons in slices: contribution of calcium conductances. J Neurophysiol 79:82–94.

Davare MA, Horne MC, Hell JW (2000) Protein phosphatase 2A is associated with class C L-type calcium channels ($Ca_V1.2$) and antagonizes channel phosphorylation by cAMP-dependent protein kinase. J Biol Chem 275:39710–39717.

Davare MA, Avdonin V, Hall DD, Peden EM, Burette A, Weinberg RJ, Horne MC, Hoshi T, Hell JW (2001) A β2 adrenergic receptor signaling complex assembled with the Ca^{2+} channel $Ca_V1.2$. Science 293:98–101.

Day M, Olson PA, Platzer J, Striessnig J, Surmeier DJ (2002) Stimulation of 5-HT_2 receptors in prefrontal pyramidal neurons inhibits Ca(v)1.2 L type Ca^{2+} currents via a PLCβ/IP3/calcineurin signaling cascade. J Neurophysiol 87:2490–2504.

Dolmetsch RE, Pajvani U, Fife K, Spotts JM, Greenberg ME (2001) Signaling to the nucleus by an L-type calcium channel-calmodulin complex through the MAP kinase pathway. Science 294:333–339.

Gao T, Yatani A, Dell'Acqua ML, Sako H, Green SA, Dascal N, Scott JD, Hosey MM (1997) cAMP-dependent regulation of cardiac L-type Ca^{2+} channels requires membrane targeting of PKA and phosphorylation of channel subunits. Neuron 19:185–196.

Gerfen CR (1992) The neostriatal mosaic: multiple levels of compartmental organization. Trends Neurosci 15:133–139.

Gomez LL, Alam S, Smith KE, Horne E, Dell'Acqua ML (2002) Regulation of A-kinase anchoring protein 79/150-cAMP-dependent protein kinase postsynaptic targeting by NMDA receptor activation of calcineurin and remodeling of dendritic actin. J Neurosci 22:7027–7044.

Graef IA, Mermelstein PG, Stankunas K, Neilson JR, Deisseroth K, Tsien RW, Crabtree GR (1999) L-type calcium channels and GSK-3 regulate the activity of NF-ATc4 in hippocampal neurons. Nature 401:703–708.

Graybiel AM (1984) Neurochemically specified subsystems in the basal ganglia. Ciba Found Symp 107:114–149.

Hell JW, Yokoyama CT, Wong ST, Warner C, Snutch TP, Catterall WA (1993a) Differential phosphorylation of two size forms of the neuronal class C L-type calcium channel alpha 1 subunit. J Biol Chem 268:19451–19457.

Hell JW, Westenbroek RE, Warner C, Ahlijanian MK, Prystay W, Gilbert MM, Snutch TP, Catterall WA (1993b) Identification and differential subcellular localization of the neuronal class C and class D L-type calcium channel alpha 1 subunits. J Cell Biol 123:949–962.

Hernandez-Lopez S, Tkatch T, Perez-Garci E, Galarraga E, Bargas J, Hamm H, Surmeier DJ (2000) D_2 dopamine receptors in striatal medium spiny neurons reduce L-type Ca^{2+} currents and excitability via a novel PLCβ1-IP3-calcineurin-signaling cascade. J Neurosci 20:8987–8995.

Hersch SM, Gutekunst CA, Rees HD, Heilman CJ, Levey AI (1994) Distribution of m1–m4 muscarinic receptor proteins in the rat striatum: light and electron microscopic immunocytochemistry using subtype-specific antibodies. J Neurosci 14:3351–3363.

Hersch SM, Ciliax BJ, Gutekunst CA, Rees HD, Heilman CJ, Yung KK, Bolam JP, Ince E, Yi H, Levey AI (1995) Electron microscopic analysis of D_1 and D_2 dopamine receptor proteins in the dorsal striatum and their synaptic relationships with motor corticostriatal afferents. J Neurosci 15:5222–5237.

Hoogland TM, Saggau P (2004) Facilitation of L-type Ca^{2+} channels in dendritic spines by activation of β2 adrenergic receptors. J Neurosci 24:8416–8427.

Howe AR, Surmeier DJ (1995) Muscarinic receptors modulate N-, P-, and L-type Ca^{2+} currents in rat striatal neurons through parallel pathways. J Neurosci 15:458–469.

Kamp TJ, Hell JW (2000) Regulation of cardiac L-type calcium channels by protein kinase A and protein kinase C. Circ Res 87:1095–1102.

Kapur A, Yeckel MF, Gray R, Johnston D (1998) L-type calcium channels are required for one form of hippocampal mossy fiber LTP. J Neurophysiol 79:2181–2190.

Kennedy MB (1998) Signal transduction molecules at the glutamatergic postsynaptic membrane. Brain Res Brain Res Rev 26:243–257.

Koschak A, Reimer D, Huber I, Grabner M, Glossmann H, Engel J, Striessnig J (2001) α1D ($Ca_V1.3$) subunits can form l-type Ca^{2+} channels activating at negative voltages. J Biol Chem 276:22100–22106.

Kreienkamp HJ (2002) Organisation of G-protein-coupled receptor signalling complexes by scaffolding proteins. Curr Opin Pharmacol 2:581–586.

Kurschner C, Yuzaki M (1999) Neuronal interleukin-16 (NIL-16): a dual function PDZ domain protein. J Neurosci 19:7770–7780.

Kurschner C, Mermelstein PG, Holden WT, Surmeier DJ (1998) CIPP, a novel multivalent PDZ domain protein, selectively interacts with Kir4.0 family members, NMDA receptor subunits, neurexins, and neuroligins. Mol Cell Neurosci 11:161–172.

Li Q, Lau A, Morris TJ, Guo L, Fordyce CB, Stanley EF (2004) A syntaxin 1, Gα(o), and N-type calcium channel complex at a presynaptic nerve terminal: analysis by quantitative immunocolocalization. J Neurosci 24:4070–4081.

Lo FS, Erzurumlu RS (2002) L-type calcium channel-mediated plateau potentials in barrelette cells during structural plasticity. J Neurophysiol 88:794–801.

Maximov A, Sudhof TC, Bezprozvanny I (1999) Association of neuronal calcium channels with modular adaptor proteins. J Biol Chem 274:24453–24456.

Mermelstein PG, Bito H, Deisseroth K, Tsien RW (2000) Critical dependence of cAMP response element-binding protein phosphorylation on L-type calcium channels supports a selective response to EPSPs in preference to action potentials. J Neurosci 20:266–273.

Murphy TH, Worley PF, Baraban JM (1991) L-type voltage-sensitive calcium channels mediate synaptic activation of immediate early genes. Neuron 7:625–635.

Platzer J, Engel J, Schrott-Fischer A, Stephan K, Bova S, Chen H, Zheng H, Striessnig J (2000) Congenital deafness and sinoatrial node dysfunction in mice lacking class D L-type Ca^{2+} channels. Cell 102:89–97.

Rajadhyaksha A, Barczak A, Macias W, Leveque JC, Lewis SE, Konradi C (1999) L-type Ca^{2+} channels are essential for glutamate-mediated CREB phosphorylation and c-*fos* gene expression in striatal neurons. J Neurosci 19:6348–6359.

Rakhilin SV, Olson PA, Nishi A, Starkova NN, Fienberg AA, Nairn AC, Surmeier DJ, Greengard P (2004) A network of control mediated by regulator of calcium/calmodulin-dependent signaling. Science 306:698–701.

Raman IM, Gustafson AE, Padgett D (2000) Ionic currents and spontaneous firing in neurons isolated from the cerebellar nuclei. J Neurosci 20:9004–9016.

Sabatini BL, Oertner TG, Svoboda K (2002) The life cycle of Ca^{2+} ions in dendritic spines. Neuron 33:439–452.

Safa P, Boulter J, Hales TG (2001) Functional properties of $Ca_V1.3$ (α1D) L-type Ca^{2+} channel splice variants expressed by rat brain and neuroendocrine GH3 cells. J Biol Chem 276:38727–38737.

Scholze A, Plant TD, Dolphin AC, Nurnberg B (2001) Functional expression and characterization of a voltage-gated CaV1.3 (α1D) calcium channel subunit from an insulin-secreting cell line. Mol Endocrinol 15:1211–1221.

Sheng M (2001) Molecular organization of the postsynaptic specialization. Proc Natl Acad Sci USA 98:7058–7061.

Sheng M, Kim E (2000) The Shank family of scaffold proteins. J Cell Sci 113:1851–1856.

Shiraishi Y, Mizutani A, Yuasa S, Mikoshiba K, Furuichi T (2004) Differential expression of Homer family proteins in the developing mouse brain. J Comp Neurol 473:582–599.

Simon M, Perrier JF, Hounsgaard J (2003) Subcellular distribution of L-type Ca^{2+} channels responsible for plateau potentials in motoneurons from the lumbar spinal cord of the turtle. Eur J Neurosci 18:258–266.

Song WJ, Tkatch T, Surmeier DJ (2000) Adenosine receptor expression and modulation of Ca^{2+} channels in rat striatal cholinergic interneurons. J Neurophysiol 83:322–332.

Surmeier DJ, Bargas J, Hemmings Jr HC, Nairn AC, Greengard P (1995) Modulation of calcium currents by a D_1 dopaminergic protein kinase/phosphatase cascade in rat neostriatal neurons. Neuron 14:385–397.

Surmeier DJ, Song WJ, Yan Z (1996) Coordinated expression of dopamine receptors in neostriatal medium spiny neurons. J Neurosci 16:6579–6591.

Tukey JW (1977) Some thoughts on clinical trials, especially problems of multiplicity. Science 198:679–84.

Vergara R, Rick C, Hernandez-Lopez S, Laville JA, Guzman JN, Galarraga E, Surmeier DJ, Bargas J (2003) Spontaneous voltage oscillations in striatal projection neurons in a rat corticostriatal slice. J Physiol (Lond) 553:169–182.

Weick JP, Groth RD, Isaksen AL, Mermelstein PG (2003) Interactions with PDZ proteins are required for L-type calcium channels to activate cAMP response element-binding protein-dependent gene expression. J Neurosci 23:3446–3456.

Wilson CJ (1993) The generation of natural firing patterns in neostriatal neurons. Prog Brain Res 99:277–297.

Wilson SM, Toth PT, Oh SB, Gillard SE, Volsen S, Ren D, Philipson LH, Lee EC, Fletcher CF, Tessarollo L, Copeland NG, Jenkins NA, Miller RJ (2000) The status of voltage-dependent calcium channels in α1E knockout mice. J Neurosci 20:8566–8571.

Xiao B, Tu JC, Worley PF (2000) Homer: a link between neural activity and glutamate receptor function. Curr Opin Neurobiol 10:370–374.

Xu W, Lipscombe D (2001) Neuronal Ca(V)1.3α(1) L-type channels activate at relatively hyperpolarized membrane potentials and are incompletely inhibited by dihydropyridines. J Neurosci 21:5944–5951.

Yan Z, Flores-Hernandez J, Surmeier DJ (2001) Coordinated expression of muscarinic receptor messenger RNAs in striatal medium spiny neurons. Neuroscience 103:1017–1024.

Yasuda R, Sabatini BL, Svoboda K (2003) Plasticity of calcium channels in dendritic spines. Nat Neurosci 6:948–955.

Zhang H, Maximov A, Xu F, Fang X, Tang T-S, Tkatch T, Surmeier DJ, Bezprozvanny I (2005) Association of $Ca_V1.3$ L-type calcium channels with Shank. J Neurosci 25:1037–1049.